JOURNAL OF GEOPHYSICAL RESEARCH, VOL. 114, A11103, doi:10.1029/2009JA014449, 2009

Excess open solar magnetic flux from satellite data: 1. Analysis of the third perihelion Ulysses pass

M. Lockwood,[1,2] M. Owens,[3] and A. P. Rouillard[1,2]

Received 12 May 2009; accepted 21 July 2009; published 12 November 2009.

[1] We use the third perihelion pass by the Ulysses spacecraft to illustrate and investigate the "flux excess" effect, whereby open solar flux estimates from spacecraft increase with increasing heliocentric distance. We analyze the potential effects of small-scale structure in the heliospheric field (giving fluctuations in the radial component on timescales smaller than 1 h) and kinematic time-of-flight effects of longitudinal structure in the solar wind flow. We show that the flux excess is explained by neither very small-scale structure (timescales < 1 h) nor by the kinematic "bunching effect" on spacecraft sampling. The observed flux excesses is, however, well explained by the kinematic effect of larger-scale (>1 day) solar wind speed variations on the frozen-in heliospheric field. We show that averaging over an interval T (that is long enough to eliminate structure originating in the heliosphere yet small enough to avoid cancelling opposite polarity radial field that originates from genuine sector structure in the coronal source field) is only an approximately valid way of allowing for these effects and does not adequately explain or account for differences between the streamer belt and the polar coronal holes.

Citation: Lockwood, M., M. Owens, and A. P. Rouillard (2009), Excess open solar magnetic flux from satellite data: 1. Analysis of the third perihelion Ulysses pass, *J. Geophys. Res.*, *114*, A11103, doi:10.1029/2009JA014449.

1. Introduction

[2] The Ulysses spacecraft is the first to survey the radial component B_r of the magnetic field in heliosphere, outside the ecliptic plane and as a function of heliospheric distance, r. It has revealed that the absolute value of the radial field (normalized to a reference r of r_1), $|B_r|(r/r_1)^2$, is independent of heliographic latitude, Λ. This was first found to apply as the satellite passed from the ecliptic plane to over the southern solar pole [*Smith and Balogh*, 1995; *Balogh et al.*, 1995]. Subsequently, this result has been confirmed by the pole-to-pole "fast" latitude scan during the first perihelion pass and during the second ascent of Ulysses to the southern polar region, as reported by *Lockwood et al.* [1999b] and *Smith et al.* [2001], respectively. The second perihelion pass has also underlined the generality of the result [*Smith and Balogh*, 2003; *Smith et al.*, 2003; *Lockwood et al.*, 2004]: this was important confirmation because, unlike the first perihelion pass, it took place under solar maximum conditions. This important result has been explained by the low plasma beta of the solar wind on leaving the coronal source surface. This results in slightly nonradial flow close to the Sun which smoothes out differences in the tangential pressure and hence renders the magnitude of the radial magnetic field constant in latitude [*Suess and Smith*, 1996; *Suess et al.*, 1996, 1998; *Lockwood*, 2004].

[3] This result means that the signed (of one radial field polarity) open solar flux threading a sphere of radius r, F_S, can be computed using

$$F_S = 2\pi r^2 \langle |B_r|_T \rangle_{CR} \quad (1)$$

The subscript CR is to denote that the averages are taken over a full Carrington Rotation, required to average out longitudinal structure. T is the timescale on which B_r data are preaveraged and then converted into absolute values. The use of $\langle |B_r|_T \rangle$, rather than $\langle B_r \rangle_T$, ensures that cancellation of opposite-polarity flux within the averaging interval T does not lead to lost flux (because in general $\langle |B_r|_T \rangle \geq |\langle B_r \rangle_T|$ and only if there is only one polarity radial flux within the averaging interval are $|\langle B_r \rangle_T|$ and $\langle |B_r|_T \rangle$ equal). The total unsigned flux through the sphere of radius r is $4\pi r^2 \langle |B_r|_T \rangle_{CR}$ and dividing this by two to obtain the signed flux (given by equation 1) assumes Maxwell's equation $\nabla \cdot \mathbf{B} = 0$ (i.e., there are no magnetic monopoles inside the heliocentric sphere of radius r). *Lockwood et al.* [2004] used data from the first two perihelion passes to show that the error introduced into F_S estimates by the use of equation (1) was less than about 5% for averages over a full CR. The value of T should be chosen so that it is not so large that the opposing field in "toward" and "away" sectors of the coronal source field are canceled (which would cause F_S to be underestimated) yet should be large enough that small-scale structure in the heliospheric field (which does not reflect structure in the source field and so would cause F_S to be overestimated)

[1]Space Environment Physics, School of Physics and Astronomy, Southampton University, Southampton, UK.
[2]Also at Space Science and Technology Department, Rutherford Appleton Laboratory, Chilton, UK.
[3]Space and Atmospheric Physics Group, Blackett Laboratory, Imperial College London, London, UK.

0148-0227/09/2009JA014449$09.00

is averaged out [*Wang and Sheeley*, 1995, 2002; *Lockwood*, 2002; *Lockwood et al.*, 2006].

[4] *Owens et al.* [2008] have recently confirmed the general validity of using equation (1) with data from a single spacecraft to compute the unsigned open solar flux ($2F_S$) by comparing the results of simultaneous observations by widely spaced craft in the heliosphere. The equation has been used with data taken from near Earth to study the long-term variation of the open solar flux [*Wang and Sheeley*, 1995; *Lockwood et al.*, 1999a; *Owens et al.*, 2008]. In turn, this has been used with historic geomagnetic data to reconstruct the variation of the open solar flux over the past 150 years [*Lockwood et al.*, 1999a; *Rouillard et al.*, 2007].

[5] The study by *Owens et al.* [2008] revealed that neither latitudinal nor longitudinal separation of heliospheric spacecraft introduced significant differences to average estimates of F_S. However, they did find a consistent (≈5% per AU) increase in the estimated F_S with heliocentric distance r, which we here refer to as the "flux excess" effect. The flux excess ΔF_S in the present paper is defined as the difference between the signed open flux F_{SU} derived using equation (1) from Ulysses data (at $r = r_U$) and F_{SA}, that at ACE (at $r = r_1 \approx 1$ AU) for the same CR. Hence

$$\Delta F_S = F_{SU} - F_{SA} = 2\pi\left\{r_U^2\langle|B_{rU}|_T\rangle_{CR} - r_1^2\langle|B_{rA}|_T\rangle_{CR}\right\} \quad (2)$$

where B_{rU} and B_{rA} are the radial fields observed by Ulysses and ACE, respectively. *Owens et al.* [2008] show that this effect becomes pronounced beyond r of about 2.5 AU and suggest an explanation is that flux estimates at large r are complicated by a reduced "signal-to-noise," where the "signal" is the radial field which reflects the source field leaving the coronal source surface of the Sun and the "noise" is small-scale structure in the radial field introduced during the field's propagation through the heliosphere (E. Smith, personal communication, 2008): as r increases, the magnetic field becomes increasingly azimuthal, increasing the uncertainty in the radial component and hence the estimated flux. In this paper we investigate the sources and nature of that "noise."

[6] In the present paper we study the third perihelion pass of Ulysses with a view to better understanding the flux excess effect. In particular, after an overview in section 2, in section 3 we look for the effects of very small-scale structure by varying the value of T used in equation (1) between 1 s and 1 h. Because this does not provide an explanation of (or even a contribution to) the observed flux excess, in section 4 we investigate the kinematic effects of the time-of-flight of plasma packets and their frozen-in magnetic field when there is longitudinal structure in the solar wind flow. Section 4 uses the theory of kinematic effects (after smoothing to remove most of the effect of dynamical stream–stream interactions in compression regions) given in the associated paper by *Lockwood et al.* [2009], which is based on the work of *Burlaga and Barouch* [1976]. Section 4.1 studies the bunching effect on solar wind plasma packet times-of-flight on the sampling by the spacecraft [*McComas et al.*, 1992], whereas section 4.2 studies the kinematic effects on the frozen-in heliospheric magnetic field. The results are compared with the effect of preaveraging the B_r data over a period of T = 1 day, which has often been adopted in the past when using equation (1) [*Wang and Sheeley*, 1995; *Lockwood et al.*, 2006].

2. Third Ulysses Perihelion Pass

[7] Figure 1 presents an overview of data from the Ulysses and ACE spacecraft during the third perihelion pass of Ulysses between day 36 of 2007 and day 13 of 2008. Figures 1f and 1g show the heliographic latitude Λ and heliocentric distance r of ACE (green line) and Ulysses (black line). Perihelion of Ulysses is at $r_U = 1.39$ AU (at $\Lambda_U = 6.9°$) and is very close to the time when Ulysses and ACE are at the same Λ. The magnitude of the longitudinal separation of Ulysses and ACE is $|\Delta\Phi| = 193.6°$ at the start of the pass, falling to 12.1° by the end of the pass (and is 97.8° at perihelion). Longitudinal structure in the corona, and in the resulting heliospheric field, means that we do not expect great similarity between ACE and Ulysses on timescales of a few days and less, and that comparisons can be made only on averages over a full solar rotation period (as seen from the craft). The solar (Carrington) Rotation period seen by Earth (and ACE) is 27.275 days and that seen by Ulysses is 26.961 days at perihelion (and 26.221 days when averaged over the whole latitude pass). We here make running means over 27.0 days intervals as we need to use an integer multiple of T (see above) when using data preaveraged on a daily basis. We use the notation that the radial field preaveraged and made into an absolute value on a timescale T and then averaged over a 27-day period is $\langle|B_r|_T\rangle_{27}$.

[8] Figure 1a shows daily means of the radial solar wind speed seen at Ulysses (V_R) and reveals an almost solar minimum configuration [*McComas et al.*, 2003] with large polar coronal holes giving uniformly fast flow, separated by a streamer belt of slower solar wind. We note, however, that coronagraph images show that the streamer belt had not reached an entirely solar minimum state at the time of this pass [*McComas et al.*, 2008]. Figure 1b presents the difference between successive daily means of V_R and shows the flow is considerably more variable on this timescale within the streamer belt. Figure 1c shows 27-day running means of all positive 1-s B_{rU} values at Ulysses (outward; red line) and all negative 1-s B_{rU} values (inward; blue line). In both cases values have been normalized to $r = r_1$ by multiplying by $(r_U/r_1)^2$. (Note that the corresponding plot for mean garden hose angles shows that for the r covered by Ulysses during this pass these are not close to 90° and so inward/outward radial field here unambiguously corresponds to toward and away field.) Like the velocity, the field also shows a near solar minimum configuration with almost zero outward field in the northern ($\Lambda > 0$) polar coronal hole and almost zero inward field in the southern ($\Lambda < 0$) polar coronal hole. The inward and outward fields are equal at the center of the streamer belt at a heliographic latitude slightly to the south of that of Earth and slightly before Ulysses and ACE are at the same Λ. Figures 4d and 4e relate to the radial field, again normalized to r_1 using the factor $(r_U/r_1)^2$. The values shown are 27-day running means for the asymptotic limit for $T \rightarrow 0$ (i.e., $\langle|B_r|_{T\rightarrow 0}\rangle_{27}$) as derived in the next section, and so do not depend on T. The "Ulysses result" of the constancy of $|B_{rU}|(r_U/r_1)^2$ with Λ is seen to apply to first order, as for the first two perihelion Ulysses passes [*Lockwood et al.*, 2004]. The ACE values (green line) show that there is a slight

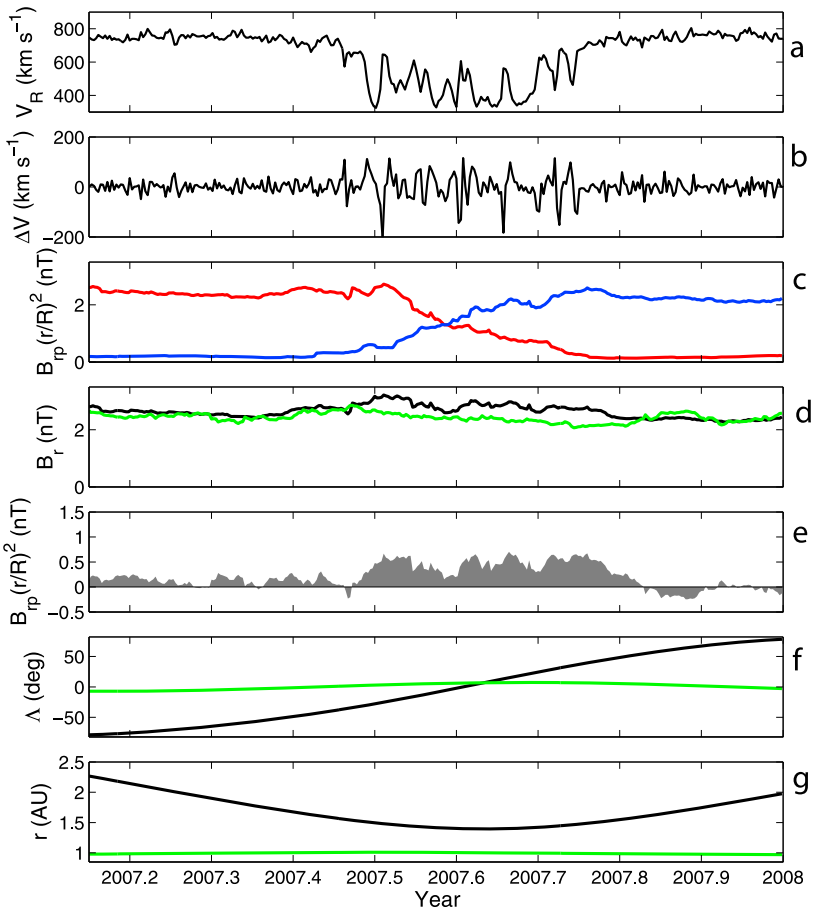

Figure 1. A comparison of Ulysses and ACE data during the third perihelion pass of Ulysses. (a) The daily means of the radial solar wind velocity observed by Ulysses, $V_{R.}$. (b) The difference between successive daily V_R values, ΔV. (c) The 27-day running means of the outward and inward (red line and blue line, respectively) radial field components observed at Ulysses, $|B_{rU}|_{out}$ and $|B_{rU}|_{in}$. (d) The 27-day running means of the normalized radial field magnitude at Ulysses, $(r_U/r_1)^2\ \langle|B_{rU}|_T\rangle_{27}$ (black line), and ACE, $\langle|B_{rA}|_T\rangle_{27}$ (green line) (e) The flux excess at Ulysses $\Delta F_S = 2\pi[r_U^2\ \langle|B_{rU}|_T\rangle_{27} - r_1^2\ \langle|B_{rA}|_T\rangle_{27}]$ (shaded area). (f) The heliographic latitude of Ulysses (Λ_U; black line) and ACE (Λ_A; green line). (g) The heliocentric distance of Ulysses (r_U; black line) and ACE ($r_A \approx r_1$; green line). In all cases the radial field values are the asymptotic values for T approaching zero, as derived in the example given in Figure 2.

decreasing trend in the near-Earth value over the interval. Outside the streamer belt, the ACE values are very close indeed to the Ulysses values but within the streamer belt there is a clear flux excess with $(r_U/r_1)^2\ \langle|B_{rU}|_{T\rightarrow 0}\rangle_{27}$ exceeding $\langle|B_{rA}|_{T\rightarrow 0}\rangle_{27}$. This flux excess ΔF_S (defined by equation (2) and calculated for the radial field estimates shown in Figure 1d) is given by the shaded area in Figure 1e. The flux excess, for these solar minimum conditions, is a phenomenon restricted to the streamer belt where the variability in solar wind flow speed is greater. This is an indication that kinematic and/or dynamical interaction effects associated with the large solar wind speed variability may be the cause of the flux excess effect noted by *Owens et al.* [2008], an idea that we investigate further in section 4.2. The mean value of the flux excess within the streamer belt (taken to be $-40° \leq \Lambda_U \leq 40°$) is $\Delta F_S = 0.59 \times 10^{14}$ Wb which is roughly 16% of the value from the ACE data at his time: $\langle r_U\rangle$ for this interval is 1.45 AU. This is very similar to the mean value found by *Owens et al.* [2008] for this *r*. Specifically, from an updated analysis of the data from all readily available sources (as presented by *Lockwood et al.* [2009, Figure 7]), the averaging bin 1.4 AU $\leq r <$ 1.5 AU yields $\langle r\rangle$ = 1.46 AU with $\langle\Delta F_S\rangle = (0.65 \pm 0.04) \times 10^{14}$ Wb (mean values, plus and minus one standard deviation). Thus the mean flux excess during this perihelion pass is typical and very close to the mean for all available data at this *r*.

3. Small-Scale Structure

[9] The need to introduce a timescale T into equations (1) and (2) means that the open flux (and hence the flux excess) will, to some extent depend on T [*Lockwood et al.*, 2006]. Hence one possibility is that very short−period fluctuations which are averaged out in the interval T in the ACE data are not similarly averaged out in the Ulysses data over the same interval, leading to an apparent flux excess.

[10] To investigate the possible effect of the smallest-scale structure (by which we here mean variations on timescales T less than an hour), 1-s radial field data (normalized to r_1 = 1 AU) from ACE and Ulysses for this third perihelion pass

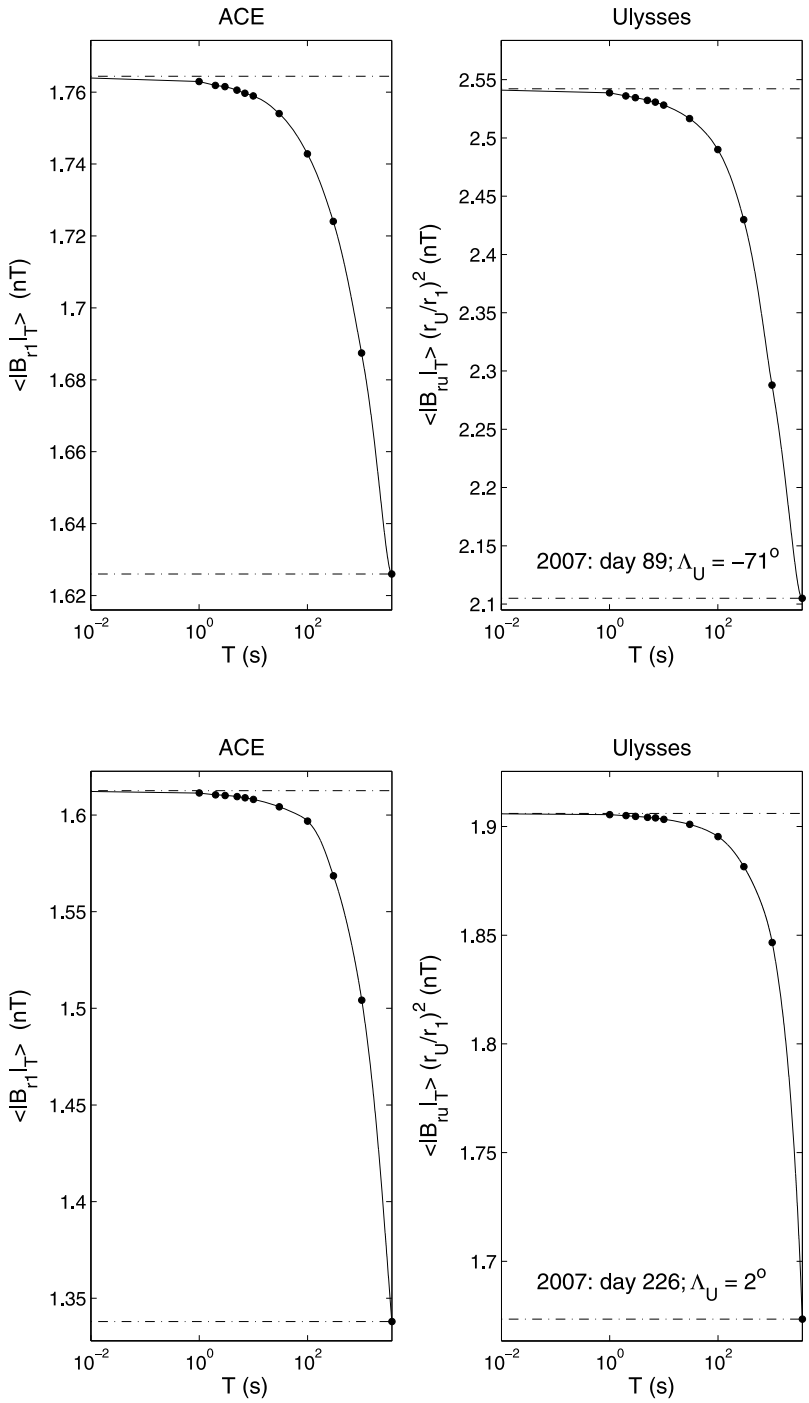

Figure 2. Analysis of the effect of averaging timescale T on 1-s radial field data from ACE and Ulysses for two example days in 2007: day 89, when Ulysses is at heliographic latitude $\Lambda_U = 71°$ and within the southern polar coronal hole, and day 224, when $\Lambda_U = 0$ and Ulysses is in the streamer belt. (left) The mean value at ACE, $\langle|B_{rA}|_T\rangle$. (right) The mean value at Ulysses, normalized to $r_1 = 1$AU, $\langle|B_{rU}|_T\rangle$ (r_U/r_1), both as a function of T. Points are for T of 1, 2, 3, 5, 7, 10, 30, 100, 300, 1000, and 3600 s, to which the solid line is a cubic spline fit. In each case the horizontal dot-dash lines are the extrapolated asymptotic limit as T approaches zero $\langle|B_r|_{T\rightarrow 0}\rangle$ and the value for $T = 1$ h, $\langle|B_r|_{T=1h}\rangle$.

were pre averaged using T of 1, 2, 3, 5, 7, 10, 30, 100, 300, 1000 and 3600 s, before absolute values being taken and daily means, $\langle|B_r|_T\rangle$, computed. The results for two example days are shown by the solid points in Figure 2. These examples (one from within a polar coronal hole, one from within the streamer belt) are typical of those for all 342 days of the pass. For both the Ulysses and the ACE data, a cubic spline was fitted to the data, as shown by the solid lines in Figure 2. The horizontal dot-dash lines show the daily means for hourly averages ($\langle|B_{rA}|_{T\,=\,1h}\rangle$ and $(r_U/r_1)^2$ $\langle|B_{rU}|_{T\,=\,1h}\rangle$ for ACE and

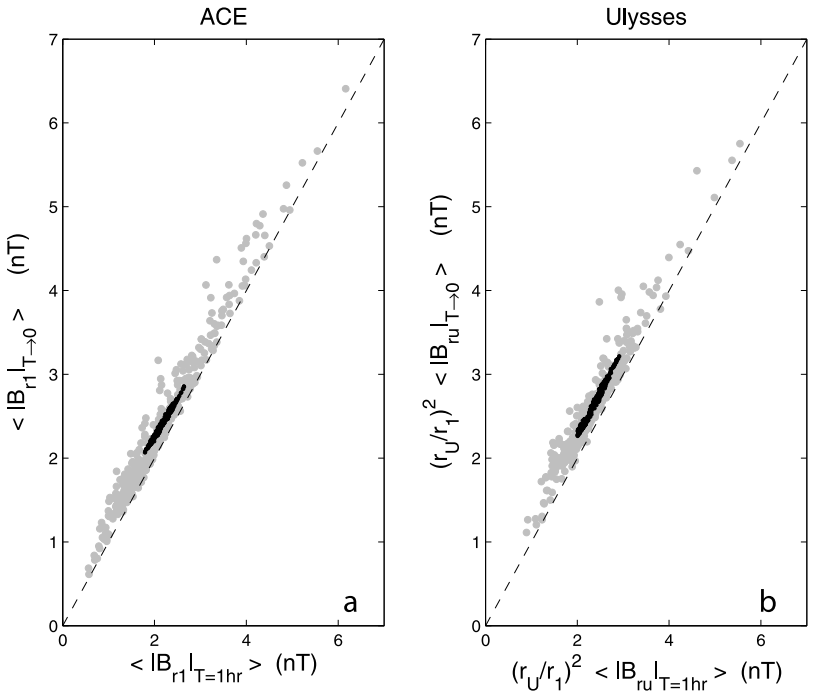

Figure 3. Scatterplots of the mean absolute radial field for $T = 1$ h against the asymptotic limiting value for $T \rightarrow 0$ (the upper horizontal dashed lines in Figure 2). Gray points are daily means, and black points are CR averages for (a) ACE data during the third Ulysses perihelion pass and for (b) the Ulysses data from the same interval. The Ulysses data have been normalized to $r = 1$ AU using the factor $(r_U/r_1)^2$. Equal values would lie on the dashed lines. The values for $T \rightarrow 0$ are systematically greater than those for $T = 1$ h by 0.23nT in Figures 3a and 3b.

Ulysses, respectively) and for the asymptotic limit where T tends to zero ($\langle |B_{rA}|_{T\rightarrow 0}\rangle$ and $(r_U/r_1)^2\ \langle |B_{rU}|_{T\rightarrow 0}\rangle$). Note that for both craft $\langle |B_r|_{T\rightarrow 0}\rangle$ is only slightly greater than the averages for the raw data used $\langle |B_r|_{T=1\ s}\rangle$ (the leftmost data points in Figure 2).

[11] The values for $T = 1$ h and $T \rightarrow 0$ are compared in the scatterplots shown Figure 3. The gray points are for daily means and the black points are for 27-day averages. The points lie consistently slightly above the dashed diagonal line showing that $\langle |B_r|_{T\rightarrow 0}\rangle$ consistent exceeds $\langle |B_r|_{T=1\ h}\rangle$. This is true for both craft, independent of the latitude of Ulysses. For both craft the difference between the two is 0.23 nT. By way of comparison, the mean flux excess in the streamer belt of $\Delta F_S = 0.6 \times 10^{14}$ Wb corresponds to an increase in $|B_r|$ at $r = r_1$ of 0.42 nT and for small-scale structure to explain the flux excess we would have needed the deviation from the dashed line in Figure 3b to have been greater than that in Figure 3a by 0.42 nT. This is clearly not the case.

[12] Thus we can conclude that there is small-scale structure in the field and it does influence the $|B_r|$ (and hence F_S) estimates depending of the T used. However, its effect is about half the radial field difference associated with the excess flux, and does not depend on either r or Λ. Because it influences both the Ulysses and the ACE data to almost exactly the same extent, we can eliminate the possibility that small-scale structure that exists at small r (but is hidden in hourly means) is "ironed out" at larger r to give the excess flux.

[13] This analysis of small-scale structure can be extended to larger timescales. However, for $T > 1$ h the behavior becomes more variable as the effects of small-scale structure in the heliosphere become convolved with other, larger-scale heliospheric effects, such as kinematic (time-of-flight) and dynamical (stream–stream interaction) effects owing to solar wind speed structure and transient events but also those of the sector structure in the source field in the solar atmosphere. Comparison of Figures 4a and 4b demonstrates the effects of using $T = 1$ day. The plot shows 27-day running means of various estimates of the absolute radial field (normalized to $r = r_1 = 1$ AU) from measurements by Ulysses and ACE during the third perihelion Ulysses pass. Values derived from ACE observations are shown by thin black lines, those from Ulysses data are shown by thick black lines. In addition, the Ulysses data in Figure 4a are also shown by the area shaded gray in Figures 4a–4c to facilitate comparisons. In Figure 4a, the variations shown are for the asymptotic limit of the timescale $T \rightarrow 0$ for which we get $\langle |B_{rA}|_{T\rightarrow 0}\rangle_{27}$ (thin line) and $(r_U/r_1)^2\ \langle |B_{rU}|_{T\rightarrow 0}\rangle_{27}$ (thick line) for ACE and Ulysses, respectively (these variations are also shown in Figure 1d). The larger values from Ulysses in the streamer belt, giving the flux excess, can be seen. Figure 1b shows the corresponding variations for $T = 1$ day: $\langle |B_{rA}|_{T\ =\ 1\ day}\rangle_{27}$ (thin line) and $(r_U/r_1)^2\ \langle |B_{rU}|_{T\ =\ 1\ day}\rangle_{27}$ (thick line). (Figure 4c is discussed in section 4.2.) It can be seen that the use of $T = 1$ day has reduced the mean values at all times. The reduction for the Ulysses data is greater in the streamer belt than for the ACE data and this means the flux excess is reduced, but not quite completely eliminated, by use of $T = 1$ day. However, early and late in the pass, Ulysses is outside the streamer belt whereas ACE remains within it: and the ACE data are lowered more by the use of $T = 1$ day than the Ulysses data at these times. It is noticeable that the lowering of the ACE data

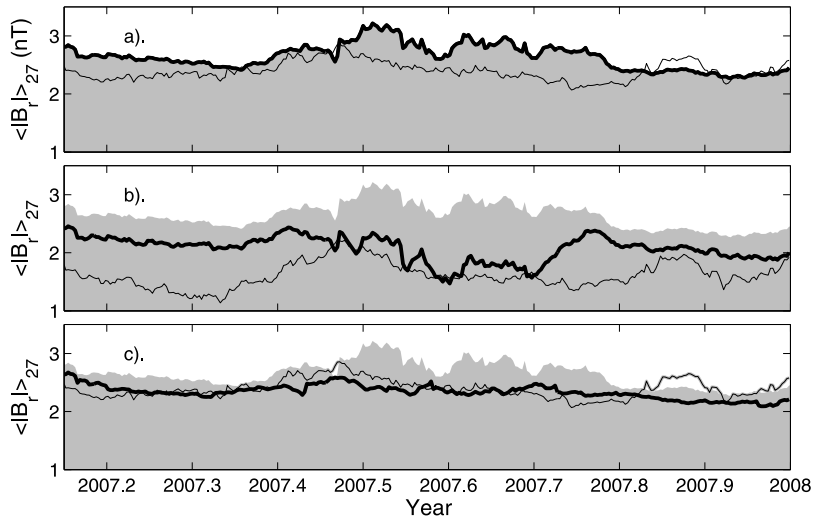

Figure 4. The 27-day running means of various estimates of the absolute radial field (normalized to $r = r_1 = 1$ AU) from measurements by Ulysses and ACE during the third perihelion Ulysses pass. Values derived from ACE observations are shown by thin black lines; those from Ulysses data are shown by thick black lines. Ulysses data are shown by the area shaded gray in Figures 4a–4c to facilitate comparisons for (a) the asymptotic limit of the timescale $T \rightarrow 0$ $\langle |B_{rA}|_{T\rightarrow 0}\rangle_{27}$ (thin black line) and $(r_U/r_1)^2$ $\langle |B_{rU}|_{T\rightarrow 0}\rangle_{27}$ (thick black line); (b) $T = 1$ day $\langle |B_{rA}|_{T\,=\,1day}\rangle_{27}$ (thin black line) and $(r_U/r_1)^2$ $\langle |B_{rU}|_{T\,=\,1\ day}\rangle_{27}$ (thick black line); and (c) the asymptotic limit $T \rightarrow 0$ with correction of the Ulysses data for the kinematic effects between r_U and r_1 (see section 3) $\langle |B_{rA}|_{T\rightarrow 0}\rangle_{27}$ (thin line) and $(r_U/r_1)^2\{\langle |B_{rU}|_{T\rightarrow 0}\rangle_{27} - \langle \Delta B_{rU}\rangle_{CR}\}$ (thick black line).

is considerably variable such that $\langle |B_{rA}|_{T\,=\,1\ day}\rangle_{27}$ has more variability than $\langle |B_{rA}|_{T\rightarrow 0}\rangle_{27}$. This contrasts with the effect for $T \leq 1$ h where the reduction is very close to constant for a given T (as in Figure 3).

[14] For the Ulysses data, the use of $T = 1$ day results in lower values within the streamer belt than in the polar coronal hole (by about the same amount that the values for $T \rightarrow 0$ are larger there). Thus using both $T = 1$ day and $T \rightarrow 0$ the Ulysses result (that $(r_U/r_1)^2$ $\langle |B_{rU}|_T\rangle_{27}$ is independent of latitude) is only a first-order result.

4. Kinematic Effects

[15] Here we use the theory of kinematic variations discussed in the work of *Lockwood et al.* [2009], which will not be repeated here. There are two effects. First field lines in compression regions are sampled more frequently than those in rarefaction regions, compared to at the source surface, and this sampling bias increases with increasing heliocentric distance r [*McComas et al.*, 1992]. In section 4.2, we investigate the potential effect of this sampling bias on the flux excess. Second, flow variations cause an additional component of the radial component of the frozen-in magnetic field [*Burlaga and Barouch*, 1976]. This effect, as discussed in section 4.2, also increases with increasing r.

4.1. Effects of Kinematic Bunching on Sampling

[16] Plasma parcels seen dt_U apart at Ulysses ($r = r_U$) will have left the sphere of radius r_1 at an intervals dt_1 apart. The velocities seen at r_U at times t_U and $(t_U + dt_U)$ are V and $V + dV$, respectively. If we assume, in the first instance, that V is independent of r (the effects of dynamic stream–stream interactions will be considered later):

$$dt_1 = dt_U + \{(r_U - r_1)/V\} - \{(r_U - r_1)/(V + dV)\} \quad (3)$$

Thus increases in the flow speed ($dV > 0$) will cause a "bunching up" of plasma parcels at Ulysses, compared to at $r = 1$ AU ($dt_1 > dt_U$) whereas if the solar wind speed decreases ($dV < 0$) this causes a relative rarefaction at the greater r ($dt_1 < dt_U$). As pointed out by *McComas et al.* [1992], spacecraft sample the heliospheric magnetoplasma at regular intervals and so at larger r they will sample the compression regions relatively more frequently than the rarefaction regions. If there is some dependence of the source $|B_r|$ on dV, this bias would have an effect on the average radial field, open flux and flux excess estimates derived from regular samples.

[17] To investigate this, we here compute the mean radial field seen by Ulysses, but also a weighted mean, $\langle |B_{rU}|\rangle_W$, in which each data point is weighted not by the (uniform) sampling interval dt_U at the spacecraft but by its corresponding interval dt_1 at $r = r_1 = 1$ AU (computed from the Ulysses data by equation (3)). Had a satellite at $r = r_1$ intersected the same solar wind as seen by Ulysses, the mean value it would have detected would have been $(r_U/r_1)^2$ $\langle |B_{rU}|\rangle_W$. The weighted mean is given by

$$\langle |B_{rU}|\rangle_W = \Sigma(dt_1/dt_U)\langle (dt_U/dt_1)|B_{rU}|\rangle. \quad (4)$$

Figure 5 shows the result for daily means: the same result is obtained for both hourly and CR means (not shown). It can be seen the effect is very small and $\langle |B_{rU}|\rangle_W$ is very close to $\langle |B_{rU}|\rangle$ at all times. The limitation to the above analysis is that the (radial) solar wind velocity V is taken to be constant between r_1 and r_U. In reality, stream–stream interaction regions will form where fast solar wind catches up with slow ahead of it [*Arge and Pizzo*, 2000]; these steepen as they propagate outward but do not generally form shocks until $r \approx 2$ AU [e.g., *Gosling*, 1996]. There are two effects which influence the bunching up of field lines in these interaction

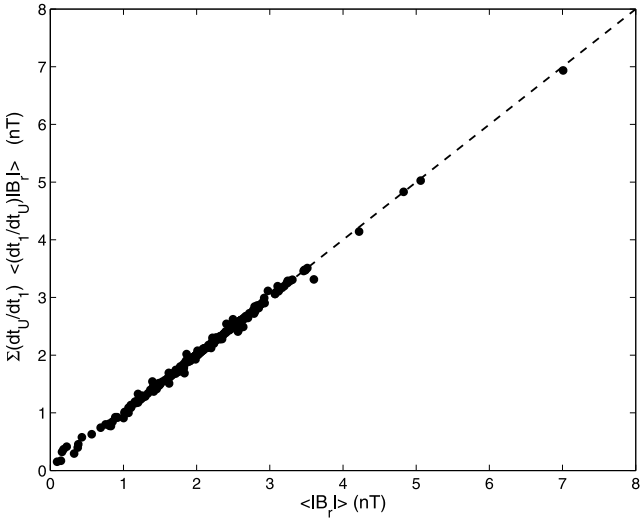

Figure 5. Scatterplot of the mean radial field over a solar rotation at Ulysses $\langle |B_{rU}| \rangle$ against the weighted mean for the same interval $\langle |B_{rU}| \rangle_W$.

regions: first the slow wind is accelerated by the fast and the fast wind is slowed by the slow wind, thus V is not constant with r. Second, the flows are deflected in direction at the interface. Quantifying the integrated effect of these dynamical effects between r_1 and r_U on (dt_1/dt_U) would require high-resolution MHD modeling. However, this effect does not occur in rarefaction regions ($dV < 0$) where fast solar wind runs ahead of slow wind and the kinematic effects can continue until the IMF is almost fully radial [*Jones et al.*, 1998; *Riley and Gosling*, 2007]. Plotting the data in Figure 5 for compression regions ($dV > 0$) and rarefaction regions ($dV < 0$) separately gives virtually identical plots to Figure 5. Thus we know dynamic effects in interaction regions are not important in this context and a sampling bias introduced by kinematic effects is not the cause of the flux excess. We have confirmed this conclusion using the theoretical modeling of kinematic structures, as developed by A. P. Rouillard and M. Lockwood (Solar stream magnetism: Analytic prediction of three-dimensional heliospheric fields and flows, submitted to *Astronomy and Astrophysics*, 2009).

4.2. Kinematic Effect on the Radial Field Magnitude

[18] *Lockwood et al.* [2009] discuss how the radial component of the magnetic field frozen into longitudinally structured flow will evolve [*Burlaga and Barouch*, 1976]. *Lockwood et al.* [2009, equation (5)] give the radial field increase, relative to its value at a reference heliocentric distance (we here use $r = r_1$), associated with a flow speed change dV

$$\Delta B_{rU} = [\partial V/\partial t]_1 \frac{(1 - r_1/r_U) B_{\varphi rU}}{\Omega V \cos \lambda_U} \qquad (5)$$

where $[\partial V/\partial t]_1$ is the temporal gradient in V at the reference surface, $B_{\varphi rU}$ is the tangential field at r_U, Ω is the angular velocity of solar rotation and λ_U is the heliographic latitude. (Note that in the work of *Lockwood et al.* [2009] the reference surface used is the coronal source surface and not that at $r_1 = 1$ AU, as is used here). Equation (3) is used to compute $[\partial V/\partial t]_1$ from the Ulysses data, using the same procedure as is used on data from $r = r_1$ in the work of *Lockwood et al.* [2009]. As in the work of *Lockwood et al.* [2009], in order to suppress dynamic stream–stream interaction effects, dV values smoothed on a 1-day timescale are used (leaving fluctuations of periods 1–27 days). Equation (5) is then used to compute hourly values of ΔB_{rU} for propagation from r_1 to r_U. The excess field for each 27-day interval $\langle \Delta B_{rU} \rangle_{27}$ was then computed, as described above, and running means of the corrected radial field $\{\langle [B_{rU}]_{T \to 0} \rangle_{27} - \langle \Delta B_{rU} \rangle_{27}\}$ are presented by the thick solid line in Figure 4c. It can be seen that this kinematic correction is small in the polar coronal hole (where $|dV|$ is low) but larger in the streamer belt (where $|dV|$ is larger). The thin line is the ACE data, as given in Figure 4a. It can be seen that the kinematic correction to the Ulysses data (from r_U back to r_1) makes it very similar to the ACE data and also gives a more constant variation with latitude than for either $T \to 0$ or $T = 1$ day. Thus the kinematic correction associated with longitudinal flow structure on timescales of 1–27 days is consistent with the flux excess observations.

5. Discussion and Conclusions

[19] This paper has investigated the flux excess observed in the third Ulysses perihelion pass and found it to be roughly consistent with the overall variation of flux excess with heliocentric distance r highlighted by *Owens et al.* [2008]. The survey of Owens et al. found the flux excess did not depend on heliographic latitude Λ because they attributed the dominant effect to r and noted that there are coherent relationships between Λ and r because of the orbit of Ulysses. This is slightly different from the results presented here where the kinematic effect is found to be larger in the streamer belt than outside it. However, we note that Owens et al.'s survey contained high-latitude data from sunspot maximum when both fast and slow flow (and hence kinematic effects) are expected at all latitudes, whereas the pass studied here was near solar minimum where the more uniform flow speeds of the large polar coronal hole give smaller kinematic effects at high latitudes. In a subsequent paper, *Lockwood and Owens* [2009] will survey the solar cycle and latitudinal dependences of the excess flux and show that they are consistent with kinematic effects.

[20] We have eliminated the possibility that small-scale structure ("roughness") of the heliosphere (defined here as giving variations in spacecraft data on preaveraging timescales T of 1 h or less) is a cause of the flux excess detected by Ulysses. The reason is that its effect is shown to be almost identical at the different heliocentric distances r sampled by Ulysses and ACE. In addition, the effect of this small-scale structure does not, unlike the flux excess in this solar minimum pass, vary with heliographic latitude, Λ. Similarly, we have shown that the time-of-flight kinematic "bunching" effect on the sampling cannot explain the excess flux detected by Ulysses. This is known because taking averages of the Ulysses data with a weighting function that allows for this bunching gives almost identical answers to taking averages over fixed intervals at the spacecraft. Dynamical effects of stream–stream interactions are not a factor because the results for compression regions and rarefaction regions are the same.

[21] Two methods of explaining and removing the excess flux seen within the streamer belt have here been found to work reasonably well. The first is using a preaveraging timescale T of about 1 day before the absolute values of the radial field are taken. The second is a kinematic correction to allow for the effect of larger-scale longitudinal flow structure on the frozen-in heliospheric field. Of these two, the kinematic correction is based on a physical analysis, albeit with some simplifying assumptions which are discussed in the work of *Lockwood et al.* [2009]. On the other hand, the use of $T = 1$ day is based on the idea that smaller-scale structure in the radial field B_r in the heliosphere does not reflect structure in the coronal source flux and should be averaged out. The choice of the T value to adopt is problematic: the use of too large a value will mean that different sectors of the source field, giving opposite polarity B_r values within the interval T, will also be averaged out and the value of $|B_r|$, and hence by equation (1) the open flux estimate will be too small. On the other hand, if too small a value for T is used not all the structure would be eliminated. The choice of T is somewhat arbitrary and does influence the F_S derived [*Lockwood et al.*, 2006]. We also note that if the source of the structure in the heliosphere is on a timescale comparable to the sector boundary crossings in the source field, there is no physical justification for using the averaging technique at all as it is not separating the source structure from the heliospheric structure (although there will be a T which would yield the true value of F_S).

[22] Taking the data from the streamer belt (here taken to be where the heliographic latitude of Ulysses is in the range $-40° \le \Lambda_U \le 40°$), the r.m.s. difference (shown in Figure 4c) between the Ulysses and ACE 27-day running means for the kinematic correction is 0.14 nT, whereas using $T = 1$ day (shown in Figure 4b) it is 0.30 nT. Thus using the kinematic correction removes (and so explains) the flux excess somewhat better than using $T = 1$ day.

[23] We here also note that the "Ulysses result" (of the constancy of the radial field component) holds better in the kinematically corrected Ulysses data in Figure 4 than for either $T = 1$ day or for $T \rightarrow 0$. The standard deviations over the whole pass of the 27-day running means the of various estimates of the absolute radial field (normalized to $r = r_1 = 1$ AU) from Ulysses are 0.22, 0.21 and 0.12 nT for $(r_U/r_1)^2 \langle |B_{rU}|_{T\rightarrow 0}\rangle_{27}$ (thick black line in Figure 4a), $(r_U/r_1)^2 \langle |B_{rU}|_{T\,=\,1day}\rangle_{27}$ (thick black line in Figure 4b) and $(r_U/r_1)^2 \{\langle [B_{rU}]_{T\rightarrow 0}\rangle_{27} - \langle \Delta B_{rU}\rangle_{27}\}$ (thick black line in Figure 4c), respectively.

[24] We should note that the origins of the two corrections are quite different. The kinematic correction allows for structure on timescales between 1 and 27 days (as it uses dV values smoothed on a 1-day timescale) whereas the $T = 1$ day correction is removing structure on timescales of 1 day and less (but is also potentially removing genuine sector structure in the source field).

[25] There is a considerable difference in the resulting corrected values of the open flux for this pass. For the kinematic correction, the mean radial field magnitude for all ACE and Ulysses data taken when Ulysses is in the streamer belt ($-40° \le \Lambda_U \le 40°$) is $|B_r| = 2.40$ nT, whereas using $T = 1$ day this value is 1.85 nT. By equation (1) these correspond to open flux estimates F_S of 3.4×10^{14} Wb and 2.6×10^{14} Wb. Thus the considerations of the flux excess in the perihelion pass of Ulysses, as presented here, have implications for the computation of open flux from observations made at r near 1 AU. *Lockwood et al.* [2009] investigate this issue.

[26] **Acknowledgments.** All three authors are supported by the UK Science and Technology Facilities Council. We are also grateful to the instrument teams of the VHM/FGM and SWOOPS instruments on the joint ESA-NASA Ulysses spacecraft and of the MAG and SWEPAM instruments on NASA's ACE mission for the provision of the data.

[27] Amitava Bhattacharjee thanks the reviewers for their assistance in evaluating this paper.

References

Arge, C. N., and V. J. Pizzo (2000), Improvement in the prediction of solar wind conditions using near-real time solar magnetic field updates, *J. Geophys. Res.*, *105*, 10,465–10,479, doi:10.1029/1999JA000262.

Balogh, A., E. J. Smith, B. T. Tsurutani, D. J. Southwood, F. J. Forsyth, and T. S. Horbury (1995), The heliospheric field over the south polar region of the Sun, *Science*, *268*, 1007–1010, doi:10.1126/science.268.5213.1007.

Burlaga, L. F., and E. Barouch (1976), Interplanetary stream magnetism: Kinematic effects, *Astrophys. J.*, *203*, 257–267, doi:10.1086/154074.

Gosling, J. T. (1996), Co-rotating and transient solar wind flows in three dimensions, *Annu. Rev. Astron. Astrophys.*, *34*, 35–73, doi:10.1146/annurev.astro.34.1.35.

Jones, G. H., A. Balogh, and R. J. Forsyth (1998), Radial heliospheric magnetic fields detected by Ulysses, *Geophys. Res. Lett.*, *25*, 3109–3112.

Lockwood, M. (2002), Relationship between the near-Earth interplanetary field and the coronal source flux: Dependence on timescale, *J. Geophys. Res.*, *107*(A12), 1425, doi:10.1029/2001JA009062.

Lockwood, M. (2004), Solar outputs, their variations and their effects on Earth, in *The Sun, Solar Analogs and the Climate*, *Saas-Fee Adv. Course*, vol. 34, edited by I. Redi, M. Güdel, and W. Schmutz, pp. 107–304, Springer, New York.

Lockwood, M., and M. Owens (2009), The accuracy of using the Ulysses result of the spatial invariance of the radial heliospheric field to compute the open solar flux, *Astrophys. J.*, *701*, 964–973, doi:10.1088/0004-637X/701/2/964.

Lockwood, M., R. Stamper, and M. N. Wild (1999a), A doubling of the Sun's coronal magnetic field during the last 100 years, *Nature*, *399*, 437–439, doi:10.1038/20867.

Lockwood, M., R. Stamper, M. N. Wild, A. Balogh, and G. Jones (1999b), Our changing Sun, *Astron. Geophys.*, *40*, 10–16.

Lockwood, M., R. B. Forsyth, A. Balogh, and D. J. McComas (2004), The accuracy of open solar flux estimates from near-Earth measurements of the interplanetary magnetic field: Analysis of the first two perihelion passes of the Ulysses spacecraft, *Ann. Geophys.*, *22*, 1395–1405.

Lockwood, M., A. P. Rouillard, I. Finch, and R. Stamper (2006), Comment on "The *IDV* index: Its derivation and use in inferring long-term variations of the interplanetary magnetic field strength" by Leif Svalgaard and Edward W. Cliver, *J. Geophys. Res.*, *111*, A09109, doi:10.1029/2006JA011640.

Lockwood, M., M. Owens, and A. P. Rouillard (2009), Excess open solar magnetic flux from satellite data: 2. A survey of kinematic effects, *J. Geophys. Res.*, *114*, A11104, doi:10.1029/2009JA014450.

McComas, D. J., J. T. Gosling, and J. L. Phillips (1992), Interplanetary magnetic flux: Measurement and balance, *J. Geophys. Res.*, *97*, 171–177, doi:10.1029/91JA02370.

McComas, D. J., H. A. Elliott, N. A. Schwadron, J. T. Gosling, R. M. Skoug, and B. E. Goldstein (2003), The three-dimensional solar wind around solar maximum, *Geophys. Res. Lett.*, *30*(10), 1517, doi:10.1029/2003GL017136.

McComas, D. J., R. W. Ebert, H. A. Elliott, B. E. Goldstein, J. T. Gosling, N. A. Schwadron, and R. M. Skoug (2008), Weaker solar wind from the polar coronal holes and the whole Sun, *Geophys. Res. Lett.*, *35*, L18103, doi:10.1029/2008GL034896.

Owens, M. J., C. N. Arge, N. U. Crooker, N. A. Schwadron, and T. S. Horbury (2008), Estimating total heliospheric magnetic flux from single-point in situ measurements, *J. Geophys. Res.*, *113*, A12103, doi:10.1029/2008JA013677.

Riley, P., and J. T. Gosling (2007), On the origin of near-radial magnetic fields in the heliosphere: Numerical simulations, *J. Geophys. Res.*, *112*, A06115, doi:10.1029/2006JA012210.

Rouillard, A. P., M. Lockwood, and I. Finch (2007), Centennial changes in the solar wind speed and in the open solar flux, *J. Geophys. Res.*, *112*, A05103, doi:10.1029/2006JA012130.

Smith, E. J., and A. Balogh (1995), Ulysses observations of the radial magnetic field, *Geophys. Res. Lett.*, *22*, 3317–3320, doi:10.1029/95GL02826.

Smith, E. J., and A. Balogh (2003), Open magnetic flux: Variation with latitude and solar cycle, in *Solar Wind Ten*, edited by M. Velli, R. Bruno, and F. Malara, pp. 67–70, Springer, New York.

Smith, E. J., A. Balogh, R. J. Forsyth, and D. J. McComas (2001), Ulysses in the south polar cap at solar maximum, *Geophys. Res. Lett.*, *28*, 4159–4162, doi:10.1029/2001GL013471.

Smith, E. J., et al. (2003), The Sun and heliosphere at solar maximum, *Science*, *302*, 1165–1169, doi:10.1126/science.1086295.

Suess, S. T., and E. J. Smith (1996), Latitudinal dependence of the radial IMF component coronal imprint, *Geophys. Res. Lett.*, *23*, 3267–3270, doi:10.1029/96GL02908.

Suess, S. T., E. J. Smith, J. Phillips, B. E. Goldstein, and S. Nerney (1996), Latitudinal dependence of the radial IMF component interplanetary imprint, *Astron. Astrophys.*, *316*, 304–312.

Suess, S. T., J. L. Phillips, D. J. McComas, B. E. Goldstein, M. Neugebauer, and S. Nerney (1998), The solar wind inner heliosphere, *Space Sci. Rev.*, *83*, 75–86, doi:10.1023/A:1005069328058.

Wang, Y.-M., and N. R. Sheeley Jr. (1995), Solar implications of Ulysses interplanetary field measurements, *Astrophys. J.*, *447*, L143–L146.

Wang, Y.-M., and N. R. Sheeley Jr. (2002), Sunspot activity and the long-term variation of the Sun's open magnetic flux, *J. Geophys. Res.*, *107*(A10), 1302, doi:10.1029/2001JA000500.

M. Lockwood and A. P. Rouillard, Space Environment Physics, School of Physics and Astronomy, Southampton University, Southampton SO17 1BJ, UK. (m.lockwood@rl.ac.uk)

M. Owens, Space and Atmospheric Physics Group, Blackett Laboratory, Imperial College London, Prince Consort Road, London SW7 2BZ, UK.